Int. J. Heat Mass Transfer. Vol. 27, No. 4, pp. 497–510, 1984
Printed in Great Britain

0017–9310/84 $3.00 + 0.00

THE EFFECTS OF THE DENSITY EXTREMUM AND BOUNDARY CONDITIONS ON THE STABILITY OF A HORIZONTALLY CONFINED WATER LAYER

LIH-TYNG HWANG,* WEN-FENG LU† and J. C. MOLLENDORF
Department of Mechanical and Aerospace Engineering, Sunyab, Amherst, NY 14260, U.S.A.

(*Received* 26 *October* 1982 *and in revised form* 17 *May* 1983)

Abstract– Using a simple non-linear density relation, the effect of the density extremum on the onset of thermal instability in a horizontally confined layer of water heated from below (at t_1) and cooled from above (at t_2) has been studied both experimentally and analytically. Both analytical and experimental results show that the density extremum has the effect of stabilizing the fluid layer. The effects of boundary conditions were also investigated. The analysis shows that realistic boundary conditions (finite thermal capacity bounding surfaces) tend to destabilize both with and without density extremum effects included. However, the qualitative behavior of Ra_c with $R = (t_m - t_2)/(t_1 - t_2)$ is relatively independent of the boundary conditions. The combined effect of both the density extremum and realistic boundary conditions is to destabilize (with respect to the Boussinesq limit of $Ra_c = 1708$) for large negative R; and to stabilize, by progressively larger amounts, as R increases. Different initial modes of instability for surface temperatures which spanned above and below 4°C were observed using a Schlieren system. The wavelengths of the observed distinct disturbance forms agree well with calculated wavelengths.

NOMENCLATURE

a	dimensionless wave number, $2\pi d/\lambda$
C	specific heat
d	spacing between surfaces or thickness of water layer
f	defined by equation (24)
F	defined by equation (21)
g	gravitational accceleration
I	electrical current in lower surface
k	thermal conductivity
p	pressure
Pr	Prandtl number, ν/α
R	dimensionless temperature excess ratio, $(t_m - t_2)/(t_1 - t_2)$
Ra	Rayleigh number, $[g\alpha(0,1)q(t_1 - t_2)\lvert t_1 - t_2\rvert^{q-1}d^3/\nu^2]\,Pr$
$q(0,1)$	1.894816
s	salinity
t	temperature
u, v, w	velocity of fluid in x, y and z direction
W	eigenfunction of velocity disturbance
x, y, z	spatial Cartesian coordinates.

Greek symbols

α	thermal diffusivity, $K/\rho C$
$\alpha(0,1)$	coefficient in density relation, $\alpha(0,1) = 9.297173 \times 10^{-6}\ \mathrm{K}^{-q}$
β	uniform adverse temperature gradient
θ	eigenfunction of temperature disturbance
λ	wavelength of initially observed disturbances
$\bar{\lambda}$	dimensionless wavelength, λ/d
μ	absolute viscosity of water
ν	kinematic viscosity of water
ρ_e	resistivity of inconel foil
ρ	density
σ	temporal growth rate of disturbance
τ	time
ϕ	dimensionless temperature disturbance.

Subscripts

1	lower boundary
2	upper boundary
c	critical, i.e. onset of motion
h	hydrostatic
m	density extremum condition
w	water
∞	ambient condition.

INTRODUCTION

WHEN a horizontal layer of a fluid with the usual monotonic density–temperature relationship is heated from below, the fluid near the lower surface expands, and thereby becomes less dense than the overlying layer. When the temperature difference exceeds a critical value, which depends on the thickness of the layer and on the properties of the fluid, the quiescent state breaks down and convection sets in. For a fluid with a non-monotonic density–temperature relationship, additional complications arise and will be discussed after a brief review of the simpler classical problem.

The problem of thermal instability in such a fluid layer heated from below is called the Bénard problem. It is recognized as an important problem in many fields of fluid motion, and is relevant to energy transport in the earth's atmosphere, its oceans, mantle and core, and the outer layer of the sun.

* Present address: Moore School of Electrical Engineering, University of Pennsylvania, Philadelphia, PA 19104, U.S.A.
† Present address: Mechanical Engineering Department, University of Minnesota, Minneapolis, MN 55455, U.S.A.

The first systematic experimental investigation of the phenomenon of the onset of thermal instability in fluids was done by Bénard in the early 1900s. He used a very thin liquid layer on a heated metallic plate and found that the fluid resolved itself into hexagonal cells.

Later, Rayleigh [1] put forward a theory which predicted the conditions under which motion first occurs, as observed by Bénard. He showed that what determined the stability of a layer of liquid heated from below was the nondimensional parameter, now called the Rayleigh number:

$$Ra = \frac{g\alpha\beta d^4}{\nu k}. \tag{1}$$

He further showed that instability arises when Ra exceeds a certain critical value (not reported by Rayleigh). It is now known that Rayleigh's theory does not apply to the system examined by Bénard since the cells visualized by Bénard were strongly influenced by surface tension effects rather than thermal convection alone. Nevertheless, Rayleigh's work is the starting point for almost all modern theories of convection, including studies concerned with density extremum and boundary condition effects such as the present investigation.

For two rigid horizontal boundaries with infinite thermal capacity, analytical studies were made by Jeffreys [2] and Low [3] following Rayleigh. Jeffreys [2] found $Ra_c = 1709.5$ at $a = 3.17$, and Low [3] found $Ra_c = 1706$. Later, the problem was done by Pellow and Southwell [4] and they arrived at $Ra_c = 1717.8$ at $a = 3.13$. Reid and Harris [5] used another approach, and got $Ra_c = 1707.8$ at $a = 3.117$. All of the above investigations considered surfaces with infinite thermal capacity and consequent total disturbance damping at the boundaries.

For a layer of water confined between two brass plates with essentially infinite thermal capacity and heated from below, experiments were done by Schmidt and Milverton [6] to verify the predicted Ra_c and to predict the instability pattern. They found the experimental Ra_c to be 1770 (average departure from this mean is 140), and observed the unstable flow pattern to be cellular motion. Experiments with an air layer have been done by Chandra [7], and the motion was made visible using tobacco smoke. He verified the criterion of stability given by Jeffreys, namely that the difference in temperature between the top and bottom of a layer, necessary to produce motion in the layer, is approximately inversely proportional to the cube of the depth. The Boussinesq approximation was used in all of the above studies.

Nevertheless, a considerably more complicated situation arises if the liquid possesses a maximum density over the temperature range being considered. For example, the linear density–temperature relationship which embodies the Boussinesq approximation cannot be accurately applied to water at low temperature. Pure water exhibits a density extremum at around 4°C at a pressure of 1 atm. Stability analysis of this problem has been carried out by Debler [8] and Tien [9] by using a parabolic density–temperature relationship:

$$\rho = \rho_m[1 - \gamma(t - t_m)^2], \tag{2}$$

where $\gamma = 8.000216 \times 10^{-6}$. Since the parabolic expression is only said to be accurate for the temperature range from 0 to 8°C, a more general density–temperature relationship:

$$\rho = \rho_m[1 - \gamma_1(t - t_m)^2 - \gamma_2(t - t_m)^3], \tag{3}$$

was presented by Sun *et al.* [10] in a study of the same problem. This expression was claimed to be accurate for a temperature up to 30°C. Merker *et al.* [11] then employed a fifth-order polynomial for a density–temperature relation. They reported that if the Ra_c calculated with the fifth-order polynomial is exact, the calculated Ra_c using the parabolic polynomial is on an average about 10% higher, and this error reduces to about 3% if a cubic term is added.

Mollendorf and Jahn [12] used a simple and accurate density–temperature relation:

$$\rho(t, s, p) = \rho_m(s, p)\{1 - \alpha(s, p)|t - t_m|^{q(s,p)}\}, \tag{4}$$

developed by Gebhart and Mollendorf [13] for both pure and saline water. The density variation is fitted in the temperature, salinity and pressure range to 20°C, 40‰ and 1000 bar absolute, respectively. Mollendorf and Jahn [12] theoretically examined the density extremum effects on the instability of a horizontally confined fluid for three different values of q, representing a wide range of salinity and pressure levels. Their calculated values of Ra_c were found to be about 10% below those of Debler [8] and Tien [9]. This is consistent with the results of Merker *et al.* [11]. A limiting situation in their calculation is the Boussinesq case ($q = 1$) for which he reported $Ra_c = 1707.8$ at $a = 3.117$.

When the bounding surfaces are not of infinite thermal capacity, disturbances are not completely damped at the boundaries. Nield [14] theoretically investigated the problem of a fluid bounded below by a rigid plate of infinite conductivity and above by a solid layer of finite conductivity and finite thickness, and took into account the effects of the slab thickness and slab thermal conductivity. As the thermal conductivity of the surface decreases, the surface is less capable of sustaining temperature gradients (in the surface) caused by temperature disturbances in the fluid. For the limiting case of $k'/k = 0$, he found that $Ra_c = 1295.8$ for $d'/d \geqslant 10$, where d', d, k' and k are slab thickness, spacing between two boundaries, thermal conductivity of the slab and thermal conductivity of the fluid, respectively.

A number of investigations concentrated on disturbance wavelength behavior. The instability pattern of a confined fluid layer with nearly infinite thermal capacity surfaces was first studied experimentally in the late 1930s. Schmidt and Saunders [15] found that the width of a cell (two adjacent rolls) was

approximately twice the layer depth when cellular motion was established. Koschmieder [16] in an experimental study found the critical wavelength to be $\bar{\lambda}_c = 2.04 \pm 0.05$, compared with the theoretical value $\bar{\lambda}_c = 2.016$ derived from linear theory by Reid and Harris [5]. More evidence of the value of critical wavelength has been found to be $\bar{\lambda}_c = 2.014$ (equivalent to $a_c = 3.12$) analytically by Mollendorf and Jahn [12]. They further provided analytical values of the critical wave number a_c for a range of temperatures, including the temperature range where the liquid possesses a maximum density.

Koschmieder [16] used a rigid lid of very poor thermal conductivity to further investigate the behavior of wavelength in another experiment. The wavelength at the onset of instability was found to be 2.16 ± 0.04, which is larger than $\bar{\lambda}_c$ for a perfectly conducting lid. This will be seen to be in agreement with the present results. He also observed that if the 'supercritical' temperature difference was applied suddenly to the fluid layer, the resulting wavelength was shorter than $\bar{\lambda} = 2.016$.

Further heat transfer and temperature measurements for fluid motion beyond Ra_c gave more insight into the complexities of the instability. Schmidt and Milverton [6] discovered that there was a sudden increase in heat transfer when the motion started. More measurements of the heat transfer through shallow layers of silicone oil, water and mercury had been made by Rossby [17]. The Nusselt number for the oil used can be written as $Nu = 0.184 Ra^{0.281}$ for $Ra > 4000$, and water follows this relation closely for $Ra < 7000$. For water at higher Rayleigh numbers, a better relationship is given by $Nu = 0.131 Ra^{0.30}$. Furthermore, the result for mercury can be approximated by $Nu = 0.147 Ra^{0.257}$ for $R > 20\,000$. Leontiev and Kirdyashkin [18] used 0.06 mm nichrome–constantan thermocouples to make temperature measurements in a cell. They measured the isotherms in the layer of fluid and found them to be wave-like, and claimed that the presence of the thermocouples did not cause any noticeable disturbances in the cell.

The present analytical study closely simulates the corresponding experiment and is described as follows. The upper surface of the fluid is adjacent to the lower side of a horizontal slab of solid copper 0.48 cm thick whose upper side consists of a heat exchanger with circulating water to keep the upper plate at essentially constant temperature. The lower boundary of the fluid is a very thin (0.013 mm thick) inconel foil which dissipates essentially constant heat flux by passing electrical current.

A Schlieren system was used to visualize the onset of motion and the subsequent flow pattern. The experiment was carried out slowly and carefully in order to maintain conditions very close to steady state. The water used was deionized and deairated with a typical electrical resistivity of 0.6 MΩ cm. A Hewlett Packard 3052A automatic data acquisition system was implemented for surface temperature measurements which were used to determine the onset of fluid motion.

THEORETICAL ANALYSIS

The usual governing equations which express the conservation of mass, momentum and energy are:

$$\frac{\partial u}{\partial x} + \frac{\partial v}{\partial y} + \frac{\partial w}{\partial z} = 0, \tag{5}$$

$$\rho\left(\frac{\partial u}{\partial \tau} + u\frac{\partial u}{\partial x} + v\frac{\partial u}{\partial y} + w\frac{\partial u}{\partial z}\right) = \mu\left(\frac{\partial^2 u}{\partial x^2} + \frac{\partial^2 u}{\partial y^2} + \frac{\partial^2 u}{\partial z^2}\right) - \frac{\partial p}{\partial x}, \tag{6a}$$

$$\rho\left(\frac{\partial v}{\partial \tau} + u\frac{\partial v}{\partial x} + v\frac{\partial v}{\partial y} + w\frac{\partial v}{\partial z}\right) = \mu\left(\frac{\partial^2 v}{\partial x^2} + \frac{\partial^2 v}{\partial y^2} + \frac{\partial^2 v}{\partial z^2}\right) - \frac{\partial p}{\partial y}, \tag{6b}$$

$$\rho\left(\frac{\partial w}{\partial \tau} + u\frac{\partial w}{\partial x} + v\frac{\partial w}{\partial y} + w\frac{\partial w}{\partial z}\right) = \mu\left(\frac{\partial^2 w}{\partial x^2} + \frac{\partial^2 w}{\partial y^2} + \frac{\partial^2 w}{\partial z^2}\right) - \frac{\partial p}{\partial z} - \rho g, \tag{6c}$$

$$\frac{\partial t}{\partial \tau} + u\frac{\partial t}{\partial x} + v\frac{\partial t}{\partial y} + w\frac{\partial t}{\partial z} = \alpha\left(\frac{\partial^2 t}{\partial x^2} + \frac{\partial^2 t}{\partial y^2} + \frac{\partial^2 t}{\partial z^2}\right). \tag{7}$$

Following the first part of the Boussinesq approximation, the density is assumed to be constant, except in the buoyancy force. The formulation proceeds, as usual, by decomposing the velocities and transport variables into base quantities and small disturbance quantities, $u = \bar{u} + u'$, $t = \bar{t} + t' = \bar{t}(z) + t'(x, y, z, \tau)$, $v = \bar{v} + v'$, $\rho = \bar{\rho} + \rho'$, $w = \bar{w} + w'$, and $p = \bar{p} + p'$ where $u' \ll \bar{u}, v' \ll \bar{v}, \ldots$, etc. Next, a temperature excess ratio is defined as

$$\phi \equiv \frac{t - t_2}{t_1 - t_2} = \frac{\bar{t} - t_2}{t_1 - t_2} + \frac{t'}{t_1 - t_2} = \bar{\phi} + \phi',$$

and from the conduction solution $\bar{\phi} = 1 - z/d$, therefore $\phi = 1 - z/d + \phi'$.

Since there is no motion in the fluid, $\bar{u} = 0$, $\bar{v} = 0$, $\bar{w} = 0$, $\bar{\rho} = \rho_h(z)$, $\bar{p} = p_h(z)$, and $-(\partial p_h/\partial z) = \rho_h g$ where the subscript h denotes local hydrostatic conditions.

After inserting the above quantities into the governing equations, and neglecting the higher order (non-linear) terms, the linearized disturbance equations are found to be

$$\frac{\partial u'}{\partial x} + \frac{\partial v'}{\partial y} + \frac{\partial w'}{\partial z} = 0, \tag{8}$$

$$\frac{\partial u'}{\partial \tau} = \mu \nabla^2 u' - \frac{\partial p'}{\partial x}, \tag{9a}$$

$$\frac{\partial v'}{\partial \tau} = \mu \nabla^2 v' - \frac{\partial p'}{\partial y}, \tag{9b}$$

$$\frac{\partial w'}{\partial \tau} = \mu \nabla^2 w' - \frac{\partial p'}{\partial z} - \rho' g, \tag{9c}$$

$$\frac{\partial \phi'}{\partial \tau} - \frac{w'}{d} = \alpha \nabla^2 \phi'. \tag{10}$$

The density equation to be used to express the buoyancy force in this analysis is the one developed by Gebhart and Mollendorf [13] for both pure and saline water, see ref. [4].

If $\rho(t)$ is expanded in a Taylor series about $\bar{\rho}$, the expression for ρ' is $\rho' = \rho_m K F \phi' |1-R|^{q-1}$, where $K = \alpha q (t_1 - t_2)|t_1 - t_2|^{q-1}$, $F = -|[(1-z/d-R)/(1-R)]|^{q-1}$, when $\bar{t} > t_m$, and $F = +|[(1-z/d-R)/(1-R)]|^{q-1}$, $\bar{t} < t_m$, where ρ_m is taken as the reference density.

Eliminating u', v', and p' from equations (9a)–(9c), one finds, in terms of w' and ϕ'

$$\left(\frac{\partial}{\partial \tau} - \nu \nabla^2\right) \nabla^2 w' = -gKF \left(\frac{\partial^2 \phi'}{\partial x^2} + \frac{\partial^2 \phi'}{\partial y^2}\right) |1-R|^{q-1}, \tag{11}$$

From equations (9a)–(9c)

$$\left(\frac{\partial}{\partial \tau} - \alpha \nabla^2\right) \phi' = w'/d. \tag{12}$$

Letting $(x, y, z)/d = x, y, z$; $w'/(\alpha/d) = w'$; $\tau/(d^2/\alpha) = \tau$, and applying the definition of Rayleigh number

$$Ra = Pr \frac{g \alpha q (t_1 - t_2)|t_1 - t_2|^{q-1} d^3}{\nu^2} |1-R|^{q-1}, \tag{13}$$

equations (11) and (12) become

$$\left(\frac{\partial}{\partial \tau} - Pr\, \nabla^2\right) \nabla^2 w' = -Ra\, Pr\, F \left(\frac{\partial^2 \phi'}{\partial x^2} + \frac{\partial^2 \phi'}{\partial y^2}\right), \tag{14}$$

$$\left(\frac{\partial}{\partial \tau} - \nabla^2\right) \phi' = w'. \tag{15}$$

Since equations (14) and (15) are linear, the solution can be written in postulated disturbance forms

$$w' = f(x, y) W(z)\, e^{\sigma \tau}, \tag{16}$$

$$\phi' = f(x, y) \theta(z)\, e^{\sigma \tau}, \tag{17}$$

where σ is the disturbance growth rate.

Plugging equations (16) and (17) into equations (14) and (15), the resulting equations are separable if

$$f_{xx} + f_{yy} + a^2 f = 0, \tag{18}$$

where a is the dimensionless wave number. Using equation (18), one can obtain

$$\left[\frac{\sigma}{Pr} - (D^2 - a^2)\right](D^2 - a^2) W = a^2\, Ra\, F \theta, \tag{19}$$

$$(\sigma - D^2 + a^2)\theta = W, \tag{20}$$

where $D \equiv d/dz$, $z = z/d$ where F, in non-dimensional form, is

$$F = \mp |[(1-z-R)/(1-R)]|^{q-1}, \tag{21}$$

which incorporates the density extremum effect. Note that for $q = 1$, $F = -1$, and density extremum effects are not included. This amounts to the Boussinesq approximation of a linear density–temperature relation. A parabolic density relation amounts to $q = 2$, and F becomes

$$F = (1-z-R)/(1-R), \tag{22}$$

which was used by Debler [8], Tien [9] and others.

The boundary conditions will be discussed after the governing equations for the copper plate and inconel foil are formulated (see Fig. 1).

The energy equation for the upper copper plate is the heat conduction equation

$$\frac{\partial^2 t_2}{\partial x^2} + \frac{\partial^2 t_2}{\partial y^2} + \frac{\partial^2 t_2}{\partial z^2} + \frac{q'''}{k_2} = \frac{1}{\alpha_2} \frac{\partial t_2}{\partial \tau}. \tag{23}$$

Decomposing, $t_2(x, y, z, \tau) = \bar{t}_2(\text{const.}) + t'(x, y, z, \tau)$, and assuming no energy generation in the copper plate, non-dimensionalizing as follows, $(x, y, z)/d = x, y, z$; $\tau/(d^2/\alpha) = \tau$, and dividing t_2' by $t_1 - t_2$, equation (23) becomes

$$\frac{\partial^2 \phi_2'}{\partial x^2} + \frac{\partial^2 \phi_2'}{\partial y^2} + \frac{\partial^2 \phi_2'}{\partial z^2} = \frac{\alpha}{\alpha_2} \frac{\partial \phi_2'}{\partial \tau},$$

where

$$\phi_2' = \frac{t_2'}{t_1 - t_2}.$$

As in equations (16) and (17), a similar assumption for ϕ_2' can be used

$$\phi_2' = f_2(x, y) \theta_2(z)\, e^{\sigma_2 \tau}.$$

Due to the no temperature slip condition between the fluid and the copper plate, f_2 must be equal to f.

By simple manipulation, it can be shown that

$$\left.\begin{aligned} f_{xx} + f_{yy} + a^2 f &= 0, \\ D^2 \theta_2 - \left(\frac{\alpha}{\alpha_2} \sigma_2 + a^2\right) \theta_2 &= 0. \end{aligned}\right\} \tag{24}$$

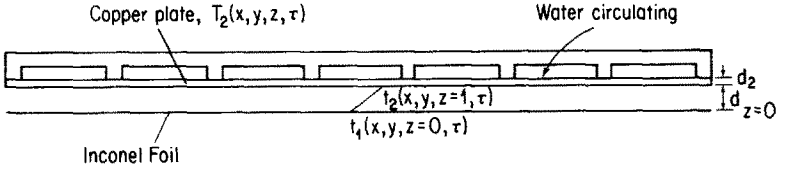

FIG. 1. Sketch of the test section, including the upper and the lower bounding surfaces.

For the lower surface (see Fig. 1) the following assumptions are believed to be reasonable:

(1) The inconel foil acts like a plane heat source, that is, no temperature gradient exists inside the foil. This is reasonable since the foil is very thin (0.013 mm thick).

(2) The foil is perfectly insulated underneath by styrofoam. This was calculated to be true to within a few percent.

At any $x, y, z = 0$

$$\frac{I^2\rho_{e1}\,dy}{d_1\,dx} = (\rho_1\,dx\,dy\,d_1)C_1\frac{\partial t_1}{\partial\tau}\bigg|_{z=0} - k_w(dx\,dy)\frac{\partial t}{\partial z}\bigg|_{z=0}. \tag{25}$$

The term on the LHS is the electrical power. The first term on the RHS accounts for the rate of energy stored in the foil. The second term is the heat flux that is conducted into the water. Perturbing t and t_1 as follows

$$t(x, y, z, \tau) = \bar{t}(z) + t'(x, y, z, \tau),$$

$$t_1(x, y, z = 0, \tau) = \bar{t}_1 + t_1'(x, y, z = 0, \tau).$$

When steady state is realized

$$\frac{I^2\rho_{e1}\,dy}{d_1\,dx} = -k_w(dx\,dy)\frac{\partial\bar{t}}{\partial z}\bigg|_{z=0},$$

and $\bar{t}_1$ is constant, equation (25) becomes

$$\rho_1 d_1 C_1\frac{\partial t_1'}{\partial\tau}\bigg|_{z=0} = k_w\frac{\partial t'}{\partial z}\bigg|_{z=0}. \tag{26}$$

But from energy conservation and the no temperature slip boundary condition, $t_1' = t'$ at $z = 0$, i.e. $f_1(x, y) = f(x, y)$ and equation (26) can be written as

$$\rho_1 d_1 C_1\frac{\partial t'}{\partial\tau}\bigg|_{z=0} = k_w\frac{\partial t'}{\partial z}\bigg|_{z=0}.$$

Letting $\tau/(d^2/\alpha) = \tau$, $z/d = z$ and dividing t' by $(t_1 - t_2)$ results in

$$\frac{\rho_1 C_1}{\rho C}\frac{d_1}{d}\frac{\partial\phi'}{\partial\tau}\bigg|_{z=0} = \frac{\partial\phi'}{\partial z}\bigg|_{z=0}.$$

Again, assuming $\phi' = f(x, y)\theta(z)\,e^{\sigma\tau}$, and substituting into the above equation yields

$$\frac{\rho_1 C_1}{\rho C}\frac{d_1}{d}\sigma\theta(0) = D\theta(0). \tag{27}$$

Since both of the boundaries are rigid, from the no velocity slip boundary condition and the continuity equation, $W(0) = W(1) = W'(0) = W'(1) = 0$. At $z = 1$, the temperature disturbance and the heat flux are continuous, so $\theta(1) = \theta_2(1)$, and $k_w D\theta(1) = k_2 D\theta_2(1)$. At $z = 1 + d_2/d$, $D\theta_2(1 + d_2/d) = 0$, since a constant temperature is maintained during the experiment.

These equations describe an eigenvalue problem, i.e. solutions for $W(z)$ and $\theta(z)$ exist for a certain combination of (σ, a, Ra). The eigenvalue, $\sigma = \sigma_r + i\sigma_i$, is a measure of the decay, or amplification, of the disturbance amplitude. The amplitudes are amplified if $\sigma_r > 0$, and are attenuated if $\sigma_r < 0$. For $\sigma_r = 0$ neutral stability results.

The principle of exchange of stabilities is valid if $\sigma_i = 0$, when $\sigma_r = 0$; i.e. the marginal states are characterized by setting $\sigma = 0$. In the Appendix, a proof that the principle of exchange of stabilities applies to the present configuration is given.

Similarly it can be shown, from equations (24), that $\sigma_2 = 0$. Substituting $\sigma = 0$, and $\sigma_2 = 0$ in the governing equations and boundary conditions results in, governing equations

$$(D^2 - a^2)^2 W = -a^2\,Ra\,F\theta, \tag{28}$$

$$(D^2 - a^2)\theta = -W, \tag{29}$$

$$(D^2 - a^2)\theta_2 = 0, \tag{30}$$

boundary conditions

$$W(0) = W(1) = W'(0) = W'(1) = 0,$$

$$\theta(1) = \theta_2(1),$$

$$D\theta(1) = KD\theta_2(1), \quad K = k_2/k_w,$$

$$D\theta(0) = 0,$$

$$D\theta_2(1 + d_2/d) = 0.$$

The well-known predictor–corrector method was used here for numerical integration. The shooting method was further employed to achieve the solution of this two point boundary value, eigenvalue problem.

THEORETICAL RESULTS AND DISCUSSION

Tables 1–3 show the calculated critical Rayleigh numbers for $q = 1.894816$, 1 and 2, respectively. In Table 1, calculations were done for three different spacings for the actual experimental thermal capacity at $q = 1.894816$. These spacings were chosen such that the temperature difference $t_1 - t_2$ could accurately be measured (to within 0.03°C). If the spacing is too large, the fluid would become unstable for a very small temperature difference. This would create a higher percentage error. If the spacing is too small, then the heat transfer capacity of the constant temperature bath for the heat exchanger would be exceeded. In the present study, three spacings were used: 0.64 and 0.85 cm for the higher temperature range, and 1.69 cm for the lower temperature range. Table 1 also shows the results of Ra_c for infinite thermal capacity and a lower value of thermal capacity (than the present experiment) for comparison purposes only.

Table 2 shows the results for calculations employing the Boussinesq approximation. From equation (28) and the definition of F, the critical Rayleigh number for Boussinesq results can be found either by setting $q = 1$ or by equating R to a large negative number. This can be seen in Table 2 and the first row of Table 1. Both values of Ra_c are very close.

The analytical curve for Ra_c vs R is presented in Fig. 2 showing the effect of thermal capacity on stability. Since

Table 1. The variation of Ra_c and a_c with R for $q = 1.894816$ for three different upper surface thermal capacities

	Actual experimental thermal capacity $k_2 = 389\ W\ m^{-1}\ K^{-1}$, copper						Hypothetical $k_2 = 0.97\ W\ m^{-1}\ K^{-1}$ glass			
	$d = 1.69$ cm		$d = 0.85$ cm		$d = 0.64$ cm		$d = 1.69$ cm		Infinite thermal capacity, from ref. [12]	
R	Ra_c	a_c	Ra_c	a_c	Ra_c	a_c	Ra_c	a_c	Ra_c	a_c
−60	1303.52	2.55	1303.87	2.55	1303.92	2.55	1021.98	1.46	1720.50	3.120
−6	1376.50	2.54	1376.86	2.55	1376.91	2.55	1082.48	1.47	1824.85	3.120
−3	1445.46	2.54	1445.84	2.54	1445.90	2.54	1140.05	1.48	1924.47	3.120
0	2260.19	2.51	2260.70	2.51	2260.77	2.51	1852.74	1.59	3172.34	3.126
0.1	2474.76	2.50	2475.28	2.50	2475.36	2.50	2052.54	1.63	3524.29	3.130
0.2	2815.73	2.49	2816.27	2.49	2816.35	2.49	2381.08	1.68	4105.10	3.140
0.3	3437.40	2.48	3437.92	2.48	3438.00	2.48	3011.21	1.79	5229.40	3.175
0.4	4835.02	2.47	4849.88	2.48	4849.93	2.48	4561.77	2.05	8030.43	3.325
0.5	9565.21	2.71	9543.05	2.70	9542.98	2.70	9888.49	2.82	17083.24	3.995
0.6	25189.80	3.79	25191.21	3.79	25191.21	3.79	25199.42	3.77	42210.35	5.095
0.7	78859.11	4.99	78859.00	4.99	78859.00	4.99	78870.02	4.99	133176.26	6.775

Table 2. Ra_c and a_c obtained using the Boussinesq approximation for three different upper surface thermal capacities

$k_2 = 389\ W\ m^{-1}\ K^{-1}$	Spacing $d = 1.69$ cm	$Ra_c = 1294.66$	$a_c = 2.55$
	Spacing $d = 0.85$ cm	$Ra_c = 1295.00$	$a_c = 2.55$
	Spacing $d = 0.64$ cm	$Ra_c = 1295.05$	$a_c = 2.55$
$k_2 = 0.97\ W\ m^{-1}\ K^{-1}$	Spacing $d = 1.69$ cm	$Ra_c = 1014.66$	$a_c = 1.46$
	Infinite thermal capacity (from ref. [12])	$Ra_c = 1707.8$	$a_c = 3.117$

the higher thermal capacity is more effective in absorbing the thermal disturbances, the higher the thermal capacity, the larger the critical Rayleigh number. This figure also shows results for the Boussinesq approximation ($q = 1$) analysis for different thermal capacities.

Figure 3 shows the variation of a_c with R for three different thermal capacities. The critical wave number a_c is higher for higher thermal capacity and lower temperature water. This shows that a poorly conducting surface results in a larger critical wavelength, which agrees with the experimental results found by Koschmieder [16]. Figure 4 shows how Ra_c changes with wave number for three different values of R for a spacing of $d = 1.69$ cm. The stability of the motionless steady state is vulnerable to disturbances at one wave number for certain values of Ra more than it is at others. For wave numbers that are either larger or smaller, a larger Ra is required to induce instability. In Fig. 4 the minimum point of each curve is called the critical wave number for the instability to occur.

Table 3. The variation of Ra_c and a_c with R for $q = 2$ for two different upper surface thermal capacities

	$k_2 = 389\ W\ m^{-1}\ K^{-1}$ Spacing $d = 1.69$ cm		Infinite thermal capacity, from ref. [12]	
R	Ra_c	a_c	Ra_c	a_c
−60			1721.87	3.120
−6			1831.16	3.120
−3			1951.39	3.120
0	2398.14	2.50	3389.84	3.126
0.1	2644.67	2.50	3797.77	3.130
0.2	3031.05	2.49	4461.31	3.140
0.3	3719.03	2.47	5715.12	3.175
0.4	5248.13	2.47	8777.68	3.325
0.5	10307.62	2.70	18662.64	3.995
0.6	27238.55	3.79	46110.15	5.095
0.7	85290.32	4.99	145509.95	6.775

In spite of the weak variation of Ra_c with d shown in Table 1, the trend of the variation is meaningful. For an upper plate thickness $d_2 = 0.48$ cm, a higher d_2/d is seen to result in a slightly larger critical Rayleigh number. Since higher d_2/d amounts to larger thermal capacity, the result is easily explained by the reasoning given above, except for $R = 0.5$. As R approaches 0.5, the effect of the density extremum evidently becomes more pronounced. When $R = 0.5$, maximum density fluid is exactly between the two surfaces and this effect appears to dominate the effect of an effective increase in the thermal capacity, at least for conditions of the present experiments.

Figure 5 shows the disturbance velocity and temperature, eigenfunctions W and θ, respectively. Both W and DW are zero at $z = 0$ and 1. The value of θ at $z = 0$ is 1, due to the normalization of the boundary condition. Table 1 shows that as k_2 decreases, the minimum critical Rayleigh number tends to decrease, i.e. it is less stable. This means that θ is a more decisive factor than W in determining the thermal instability.

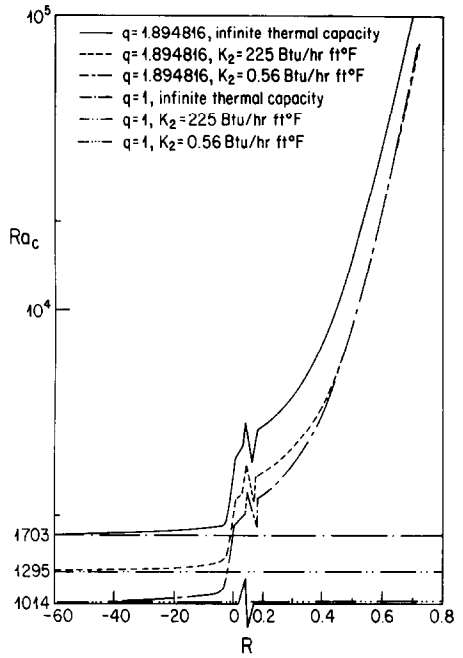

FIG. 2. The variation of Ra_c with R for $q = 1.894816$ and 1 (Boussinesq approximation), each for three different upper surface thermal capacities.

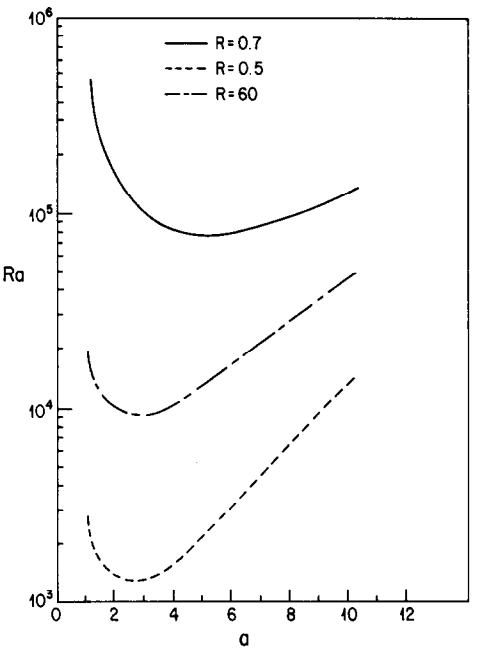

FIG. 4. The calculated variation of Ra with a for $k_2 = 389$ W m^{-1} K^{-1}, $d = 1.69$ cm and $q = 1.894816$ for three values of R.

EXPERIMENT

The layout of the experimental apparatus is shown in Fig. 6. Thermocouples are connected to the upper and lower boundaries of the layer of water. The Schlieren system is used for flow visualization.

The test section shown in Fig. 7 is placed in a 71 × 69 × 91 cm tank filled with purified water. The reason for using a large tank is to prevent close interaction between the test section and the atmosphere, especially when the test section is at a low temperature. The layer of water to be tested has dimensions of 47.8 × 29.2 × d cm. The heat generated electrically in the lower surface is removed by the circulating water in the upper plate heat exchanger, which also maintains conditions fairly close to constant temperature within the copper plate. The average deviation from mean temperature in the plate was approximately 0.05°C. The four sides of the layer are bounded by Plexiglas to prevent entrainment of water. The surface temperatures are measured using thermocouples, which are embedded in the copper

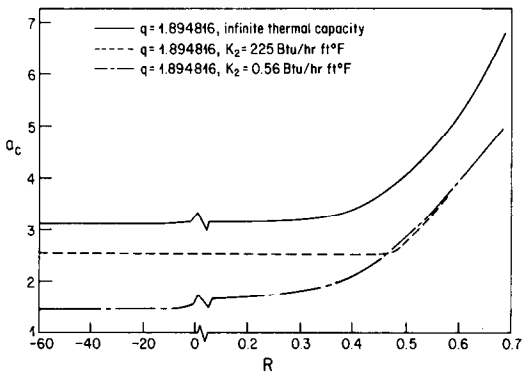

FIG. 3. The variation of a_c with R for $q = 1.894816$ for three different upper surface thermal capacities.

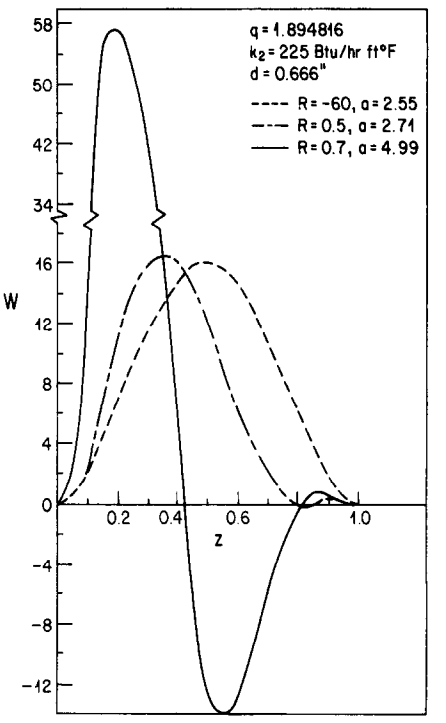

FIG. 5(a). The variation of the disturbance velocity eigenfunction, W, with z for three different values of R.

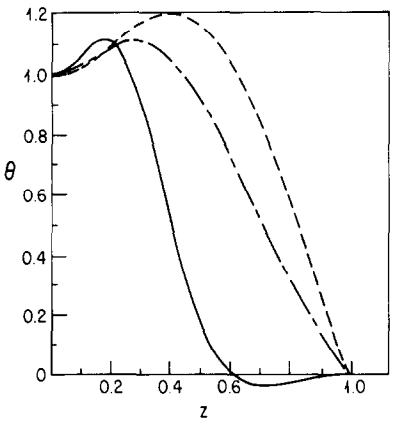

FIG. 5(b). The variation of the disturbance temperature eigenfunction, θ, with z for three different values of R.

plate and beneath the inconel foil, see Fig. 8. A dial indicator (accurate to 0.025 mm), which is positioned on the top of the tank, is used to measure the distance between the two boundaries. Thirty-six gauge chromel–alumel thermocouples (with positive chromel wires and negative alumel wires) were used in this experiment.

The thermocouple junction beads in the copper plate are coated with glyptol and potted in silver epoxy. The glyptol coating prevents a short circuit between the thermocouple junctions. The silver epoxy is to assure a good thermal contact between the junction and the surface of the copper plate. The thermocouple junction beads at the lower boundary are covered with a layer of 0.025 mm thick mylar, which is placed beneath the inconel foil to avoid short circuiting. The silicone grease in between the styrofoam, mylar and inconel foil

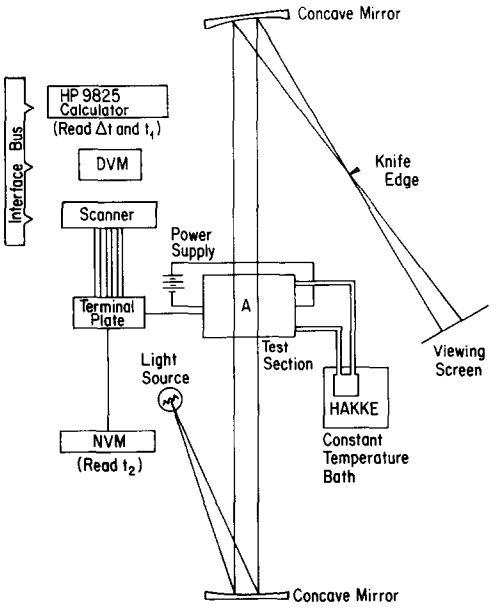

FIG. 6. The layout of the experimental apparatus.

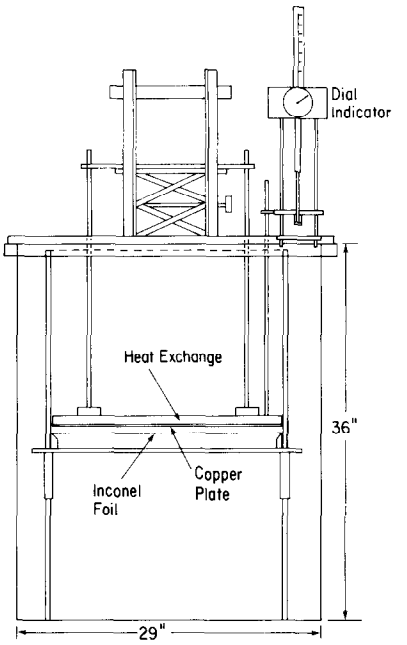

FIG. 7. The arrangement of the test section in the water tank.

serves to enhance thermal contact and results in more reliable temperature measurement.

The main purposes of the experiment are to compare the experimental results with the theoretical calculation of the critical Rayleigh number and to observe the flow pattern at the onset of instability of a layer of water. The temperature difference and spacing between the upper and lower boundaries are the two experimental parameters. Before each run, the spacing between the two boundaries was set, and the Schlieren system was aligned. The knife edge was adjusted to achieve the optimum compromise between light intensity and contrast. The ambient water temperature was made uniform by stirring the tank contents at frequent intervals preceding a run. The stirrer was stopped at least 2 h before the start of each experimental run to allow any disturbances and circulations to damp out. After the water in the tank was quiescent, the circulator was switched on to drive the cooling water (which had a slightly lower temperature than the water in the tank) into the heat exchanger. When the temperature of the upper and lower boundaries were approximately equal, the power supply was turned on.

Since steady state was desired in this study, the current passed through the inconel foil was increased *very* slowly and carefully. The change in current was as small as 0.1 A. The current was changed only after the layer of water reached a quiescent state.

The circulator, which supplied the water to the heat exchanger and maintained a constant upper surface temperature, was able to keep the thermocouple voltage variation of t_2 within $\pm 2\ \mu$V, i.e. 0.05°C. The flow rate in the circulator and heat exchanger was normally increased by adjusting the control valve when the heat generated from inconel foil was higher.

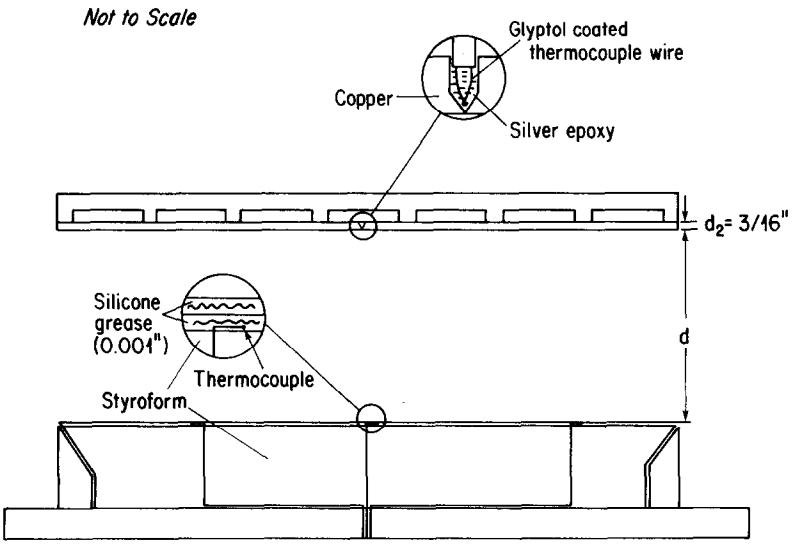

FIG. 8. Location and placement of the thermocouples in each bounding surface.

The Schlieren system was not used to determine the onset of motion since it is dependent on the sensitivity of the system, and furthermore, the flow pattern normally became visible slightly after the onset of motion, as determined by the temperature history of two boundaries. Although it is, therefore, not very suitable to detect the very beginning of the onset of motion, it is useful for subsequent flow visualization. Several photographs were taken after the flow pattern was established. If the lower surface temperature kept increasing, the flow pattern in the layer of water would change gradually. The wavelength of the pattern was also measured as close to the onset of motion as possible.

Most of the experiments were performed late at night to avoid any large disturbances caused by daytime activity in the building.

EXPERIMENTAL RESULTS AND DISCUSSION

Two different groups of temperature ranges were used in the experiment to check: (1) the effects of boundary conditions and (2) the effects of density extremum on the instability of a horizontally confined water layer. The boundary condition effects were checked at the higher temperature range where density extrema effects are minimal. Here the critical Rayleigh number is 1295, compared with 1708 for surfaces of infinite thermal capacity. This shows that the finite thermal capacity of the boundaries has the effect of destabilizing the water layer. The density extremum effects were checked at temperatures around 4°C where they are most pronounced. Theoretical results predict that density extremum effects cause Ra_c to increase with lower surface temperatures, which indicates that the density extremum has the effect of stabilizing the water layer.

If the electrical power increase at the lower surface was not done carefully and slowly, 'mushroom-like' thermals were observed throughout the experiments. As these were avoided it suggests that the experiments met the quasi-static requirement, because a thermal is known to be formed under an unsteady heating process, see Sparrow *et al.* [19].

Two methods were proposed here to determine the onset of instability. One is determined directly by the temperature history of the surfaces. In the pure conduction mode, the temperature difference between the two surfaces will increase linearly with the power supply to the foil. The sudden drop in temperature difference between the two surfaces indicates that convective motion has started. From this, a measurement of the surface temperatures provided a means for determining the onset of motion.

The second method is determined by graphs of the variation of the lower surface temperature with the square of the current. One could determine the onset of instability from such a graph at the point when experimental data indicates a departure from the linear relationship between temperature and I^2. This means convection sets in at the point when the slope of the linear relationship of the lower surface temperature and I^2 changes.

The experimental results obtained using these two criteria for determining the onset of motion are shown in Tables 4 and 5. The *maximum* deviation from predictions of Ra_c is 18.56% using criterion 1 and 22.36% using criterion 2. The *average* deviation is 8.56 and 9.24% using criterion 1 and 2, respectively. The comparisons of experimental values of Ra_c with the theoretical curve are also shown in Figs. 9 and 10. These show good agreement between experimental data and theoretical values. It seems clear from the experimental values of Ra_c that the density extremum effect has a

Table 4. Experimental data determined by criterion 1

Expt. No.	Spacing (in.)	t_2 (μV)	t_2 (°C)	t_1 (μV)	t_1 (°C)	R	Ra_c	Estimated deviation Ra_c (%)
1	0.25	859	21.51	873	21.85	−51.29	1409.90	6.74
2	0.25	831	20.84	846	21.20	−48.05	1393.70	5.98
3	0.33	544	13.67	554	13.92	−38.70	1226.90	7.82
4	0.25	645	16.20	675	16.87	−27.05	1239.91	7.53
5	0.25	628	15.77	646	16.22	−26.16	1171.10	12.93
6	0.20	506	12.72	567	14.25	−7.09	1262.11	7.87
7	0.33	300	7.57	325	8.20	−5.67	1231.60	10.10
8	0.33	259	6.25	296	7.47	−2.70	1490.21	2.30
9	0.66	184	4.65	199	5.02	−1.65	1508.94	15.23
10	0.66	165	4.17	190	4.80	−0.22	2139.87	0.93
11	0.66	158	4.00	189	4.77	0.30	2560.13	10.15
12	0.66	157	3.97	192	4.85	0.06	2485.72	5.30
13	0.66	153	3.87	191	4.82	0.21	2952.05	1.79
14	0.66	147	3.72	202	5.10	0.27	3783.46	15.68
15	0.66	141	3.55	190	4.80	0.35	4722.61	13.79
16	0.66	137	3.46	197	4.97	0.38	5394.79	18.56
17	0.66	132	3.33	197	4.97	0.41	6477.20	27.00
18	0.66	122	3.07	205	5.17	0.47	8075.57	4.65
19	0.66	109	2.75	212	5.35	0.52	10996.46	9.86
20	0.66	88	2.23	212	5.35	0.57	16488.70	10.87
21	0.66	74	1.88	220	5.55	0.58	21952.90	5.03
22	0.66	50	1.25	224	5.65	0.61	27890.77	7.34

tendency to stabilize the water layer since Ra_c is larger when the density extremum becomes significant.

The unstable flow pattern, seen using the Schlieren system, gradually appeared after the actual onset of motion. The pattern observed depends strongly on the geometry of the experimental apparatus. Since the preferred mode of convection between horizontal plates is known to be a series of two-dimensional periodic roll-shaped cells whose axes are parallel to the short side of the plate, a well organized periodic pattern is expected here between the two boundaries. A slightly irregular pattern, observed in some experiments, is thought to be caused by non-uniformities in the temperature of the boundaries. It is known that controlled initial conditions may be employed to obtain a regular pattern of steady convection rolls. When the Rayleigh number is increased further and reaches a value somewhat larger than many times its critical value, the two-dimensional rolls change into a three-dimensional form.

It is assumed here that the fundamental configuration of the pattern seen here consists of rolls, which have a long tubular form. Since the repeating unit in the pattern consists of two rolls rotating in opposite direction, the wavelength of the pattern is defined as the width of the two rolls.

Table 5. Experimental data determined by criterion 2

Expt. No.	Spacing (in.)	t_2 (μV)	t_2 (°C)	t_1 (μV)	t_1 (°C)	R	Ra_c	Estimated deviation Ra_c (%)
2	0.25	831	20.84	846	21.20	−48.05	1393.70	5.98
4	0.25	645	16.20	675	16.87	−27.05	1239.91	7.53
6	0.20	506	12.72	567	14.25	−7.09	1262.11	7.87
7	0.33	300	7.57	323	8.15	−5.91	1176.41	13.11
8	0.33	259	6.52	289	7.30	−3.14	1240.04	12.67
9	0.66	184	4.65	199	5.02	−1.65	1508.94	15.23
10	0.66	165	4.17	189	4.77	−0.23	1999.71	6.99
11	0.66	158	4.00	189	4.77	0.03	2560.13	10.15
12	0.66	157	3.97	192	4.85	0.06	2485.72	5.30
13	0.66	153	3.87	190	4.80	0.22	2628.11	11.22
14	0.66	147	3.72	200	5.05	0.29	3411.22	2.50
15	0.66	141	3.55	191	4.82	0.37	4313.45	1.49
16	0.66	137	3.46	196	4.95	0.38	5567.68	22.36
18	0.66	122	3.07	201	5.07	0.48	7816.40	2.29
19	0.66	109	2.75	209	5.27	0.51	12161.20	15.82
22	0.66	50	1.25	224	5.65	0.61	27890.77	7.34

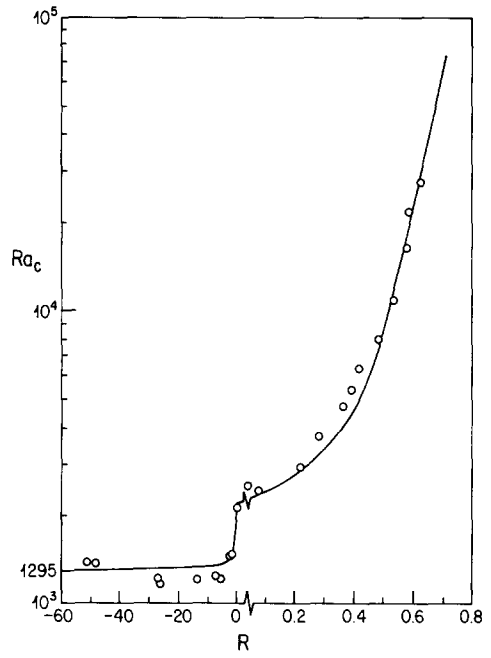

FIG. 9. Comparison of theoretical and experimental variation of Ra_c with R for criterion 1.

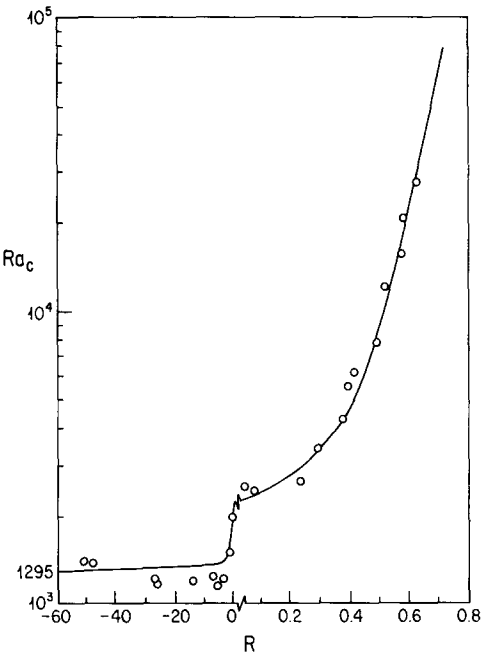

FIG. 10. Comparison of theoretical and experimental variation of Ra_c with R for criterion 2.

The wave number has been defined by many investigators in this problem as 2π times the layer depth divided by observed roll width. It is believed that instability sets in earliest for a particular wave number. The sensitivity of the fluid to disturbances at a particular wavelength implies that those disturbances will be amplified sooner than any others when the layer becomes unstable. Therefore the pattern observed when convection begins might be expected to have disturbances of about this wavelength.

A determination of the precise physical meaning of the nondimensional critical wavenumber requires a solution of equation (18). This further requires a postulated disturbance form. Experimental findings depend upon many factors, most notably the shape and relative extent of the boundaries of the fluid layer. The present experimental Schlieren observations provide only an integrated view through the water layer along the light path. A view from the top was not possible with the present experimental apparatus. Nevertheless, the distinct periodicity shown in the Schlieren photographs suggests a dominant periodic unstable pattern in one direction. Therefore it seems reasonable to assume that $f = e^{i(KxX + KyY)}$, see Chandrasekhar [20], and that $Kx \approx 0$. Then $Ky = 2\pi/\lambda$ and $a = 2\pi d/\lambda$.

Table 6 shows a comparison between the analytical and experimental critical wavelength. They agree well with each other. The average deviation of the experimental critical wavelength from the analytical critical wavelength is 7.39%. This good agreement

Table 6. Comparison of calculated and experimentally determined critical wavelength

R	Spacing (cm)	$A_{c,analy.}$	$\lambda_{analy.}$ (cm)	$a_{c,expt.}$	$\lambda_{c,expt.}$ (cm)	Deviation λ_c (%)
−51.29	0.64	2.55	1.57	2.45	1.63	3.22
−38.70	0.85	2.55	2.06	2.30	2.31	12.34
−26.16	0.64	2.55	1.57	2.45	1.63	3.22
−5.67	0.85	2.54	2.08	2.41	2.18	4.87
−2.70	0.85	2.54	2.08	2.51	2.11	1.22
−0.22	1.69	2.51	4.19	2.61	4.04	3.64
0.03	1.69	2.51	4.19	2.92	3.61	13.94
0.06	1.69	2.51	4.19	2.63	4.01	4.24
0.21	1.69	2.49	4.22	2.59	4.06	3.61
0.27	1.69	2.48	4.24	2.66	3.96	6.58
0.41	1.69	2.48	4.24	3.15	3.33	21.56
0.52	1.69	2.92	3.61	3.24	3.25	9.86
0.57	1.69	3.30	3.20	3.70	2.84	11.11
0.58	1.69	3.40	3.10	3.80	2.77	10.64
0.61	1.69	3.91	2.69	3.93	2.67	0.94

seems to be a vindication of the assumptions made above.

An example of the photographic results of the unstable flow patterns are shown in Figs. 11(a)–(d) and 12(a)–(c). For $R < 0$, the development of the unstable patterns are shown in Figs. 11(a) and (b). For $0 < R < 0.5$, Fig. 11(c) shows the flow pattern in this group. An approximate periodic pattern can be seen from one end to the other end of the layer. Sidewall effects do not appear to be a predominant factor since the aspect ratio is high in the experiment. For $0.5 < R < 1$, Fig. 11(d) shows the flow pattern which developed. It is believed that the 'egg shape' pattern appeared near the lower boundary because the density extremum is below the center line of the layer for $0.5 < R < 1$.

Figures 12(a)–(c) show the random pattern of flow which results when Ra is increased to a value of 89 times Ra_c. The flow is unstable to many kinds of disturbances, and is unsteady. The flow is then believed to be quite chaotic, and the rolls appear to be totally unstable.

CONCLUSIONS

The experimental values of Ra_c are within an average of 8.9% deviation from analytical values using two criteria to determine the onset of motion. The formation of an unstable pattern on the Schlieren viewing screen is believed not to be as accurate as the other two criteria for determining Ra_c since the flow pattern normally becomes observable slightly after the onset of motion. The methods used here to determine the onset of motion are from the temperature history of the bounding surfaces.

The present study not only compares the experimental values of Ra_c with the corresponding analysis, but also visualizes the unstable convective pattern. A Schlieren system is found to be convenient for this. The observed pattern is believed to be composed of rolls with tubular form which are parallel to the short side of the layer. The experimental values of wavelength are within an average of 7.39% deviation from analytical values.

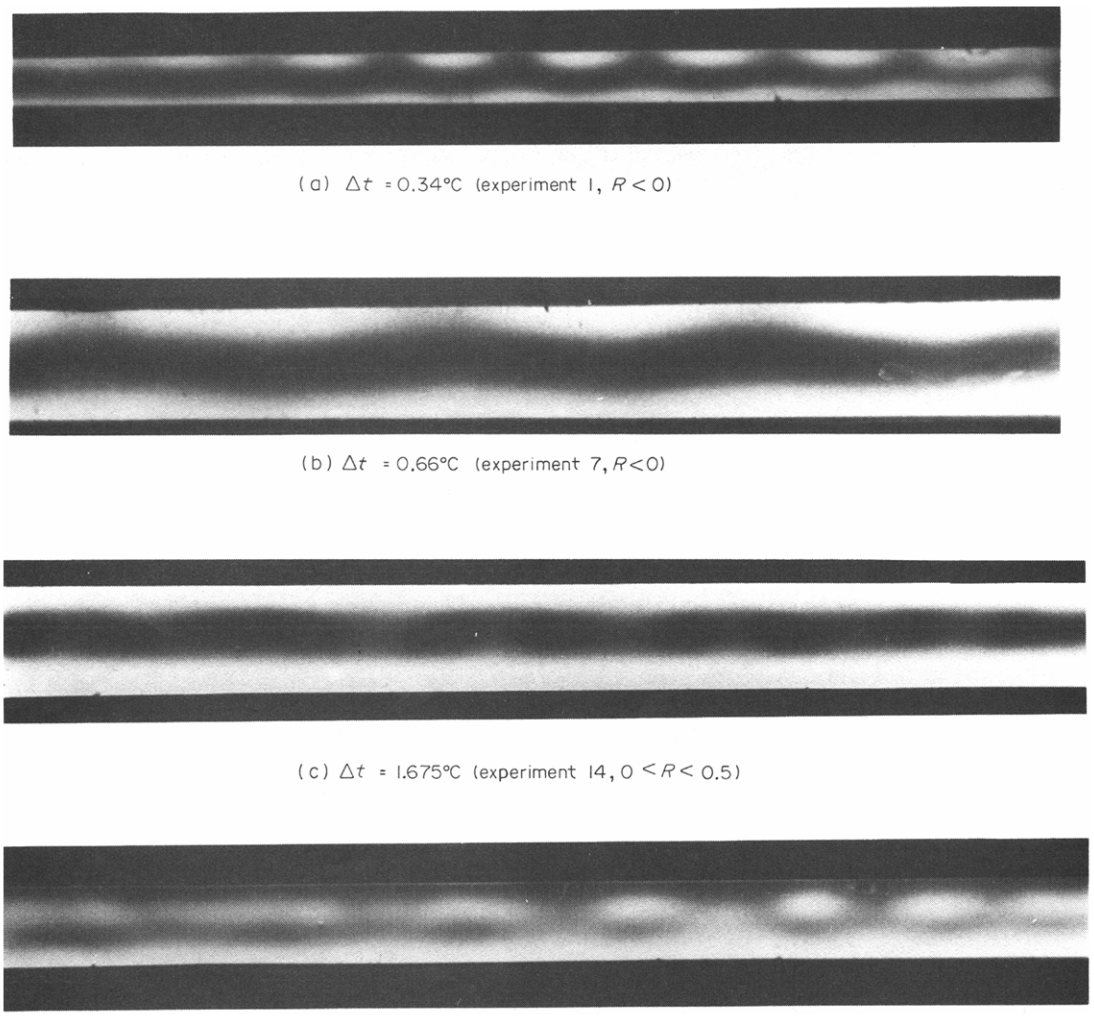

FIG. 11. Unstable flow pattern for experiments 1, 7, 14, and 21.

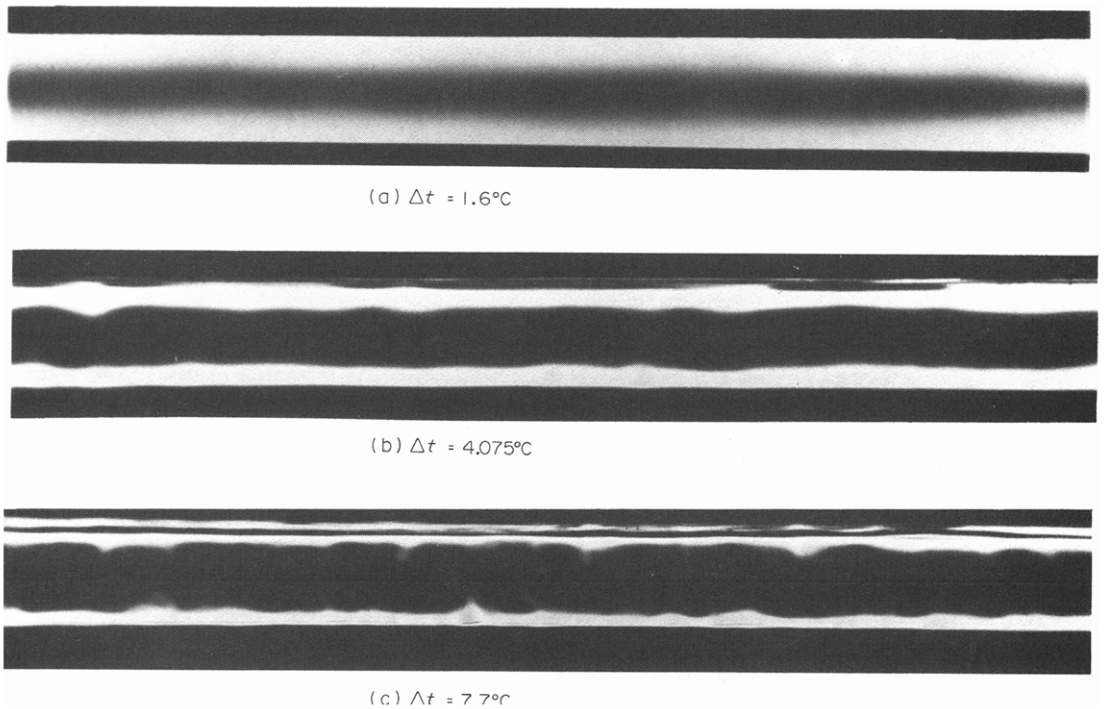

FIG. 12. Sequential development of unstable flow pattern for experiment 12.

Acknowledgements—The authors gratefully acknowledge support for this research from the National Science Foundation (ENG7727945), the construction of experimental apparatus by Mr Harold Wagner and excellent typing by Kay Ward and Elaine Sokolowski.

REFERENCES

1. Lord Rayleigh, On convection currents in a horizontal layer of fluid when the higher temperature is on the under side, *Phil. Mag. J. Sci.* **32** (192), 529–546 (1916).
2. H. Jeffreys, Some cases of instability in fluid motion, *Proc. R. Soc.* **A118,** 195–208 (1928).
3. A. R. Low, On the criterion for stability of a layer of viscous fluid heated from below, *Proc. R. Soc.* **A125,** 180–195 (1929).
4. A. Pellow and R. V. Southwell, On maintained convective motion in a fluid heated from below, *Proc. R. Soc.* **A176,** 312–343 (1940).
5. W. H. Reid and D. L. Harris, Some further results on the Bénard problem, *Physics Fluids* **1**(2), 102–110 (1958).
6. R. J. Schmidt and S. W. Milverton, On the stability of a fluid when heated from below, *Proc. R. Soc.* **A152,** 586–594 (1935).
7. K. Chandra, Instability of fluids heated from below, *Proc. R. Soc.* **A164,** 231–242 (1938).
8. W. R. Debler, On the analogy between thermal and rotational hydrodynamic stability, *J. Fluid Mech.* **24,** 165–176 (1966).
9. C. Tien, Thermal instability of a horizontal layer of water near 4°C, *A.I.Ch.E. Jl* **14,** 652–653 (1968).
10. Z. S. Sun, C. Tien and Y. C. Yen, Thermal instability of a horizontal layer of liquid with maximum density, *A.I.Ch.E. Jl* **15,** 910–915 (1969).
11. G. P. Merker, P. Waas and U. Grigull, Onset of convection in a horizontal water layer with maximum density effect, *Int. J. Heat Mass Transfer* **22,** 505–515 (1979).
12. J. C. Mollendorf and K. H. Jahn, Onset of convection in a horizontal layer of cold water, *Am. Soc. Mech. Engrs*, Series C, *J. Heat Transfer* **105,** 460–464 (1983).
13. B. Gebhart and J. C. Mollendorf, A new density relation for pure and saline water, *Deep Sea Res.* **24,** 831–848 (1977).
14. D. A. Nield, The Rayleigh–Jeffreys problem with boundary slab of finite conductivity, *J. Fluid Mech.* **32,** 393–398 (1968).
15. R. J. Schmidt and O. A. Saunders, On the motion of a fluid heated from below, *Proc. R. Soc.* **A165,** 216–228 (1938).
16. E. L. Koschmieder, On the wavelength of convective motions, *J. Fluid Mech.* **35,** 527–530 (1969).
17. H. T. Rossby, A study of Bénard convection with and without rotation, *J. Fluid Mech.* **36,** 309–335 (1969).
18. H. Leontiev and A. G. Kirdyashkin, Experimental study of flow patterns and temperature fields in horizontal free convection liquid layers, *Int. J. Heat Mass Transfer* **11,** 1461–1466 (1968).
19. E. M. Sparrow, R. B. Husar and R. J. Goldstein, Observations and other characteristics of thermals, *J. Fluid Mech.* **41,** 793–800 (1970).
20. S. Chandrasekhar, *Hydrodynamic and Hydromagnetic Stability*. Clarendon Press, Oxford (1961).

APPENDIX

Letting $\sigma = 0 + \mathrm{i}\sigma_i$, $\theta = \theta_r + \mathrm{i}\theta_i$, $\mathrm{W} = \mathrm{W}_r + \mathrm{i}W_i$, and substituting these into equation (20),

$$D^2\theta_r = a^2\theta_r - \sigma_i\theta_i - W_r,$$

$$D^2\theta_i = \sigma_i\theta_r + a^2\theta_i - W_i,$$

or

$$\begin{bmatrix} \ddot{\theta}_r \\ \theta_i \end{bmatrix} = \begin{bmatrix} a^2 & -\sigma_i \\ \sigma_i & a^2 \end{bmatrix} \begin{bmatrix} \theta_r \\ \theta_i \end{bmatrix} - \begin{bmatrix} W_r \\ W_i \end{bmatrix},$$

where $\sigma_r, \theta_r, \theta_i, W_r$ and W_i are real. This system of equations can further be simplified as

$$\dot{X} = AX + C,$$

where

$$X = \begin{bmatrix} \theta_r \\ \theta_i \end{bmatrix}, \quad A = \begin{bmatrix} a^2 & -\sigma_i \\ \sigma_i & a^2 \end{bmatrix}, \quad \text{and } C = -\begin{bmatrix} W_r \\ W_i \end{bmatrix}.$$

The solution above can be found by adding a homogeneous solution to a particular solution. If the homogeneous solution has the form $X_h = Y e^{\gamma z}$, then the homogeneous equation becomes

$$(A - \gamma I)Y = 0,$$

where $\lambda = \gamma^2$, and I is the unit matrix. In order to get a nontrivial solution, the determinant of $(A - \lambda I)$ should be equal to 0, i.e.

$$\begin{vmatrix} a^2 - \lambda & -\sigma_i \\ \sigma_i & a^2 - \lambda \end{vmatrix} = (a^2 - \lambda)^2 + \sigma_i^2 = 0.$$

Solving for λ, one gets $\lambda = a^2 \pm i\sigma_i$. But θ_r and θ_i must be real, and $\lambda = \gamma^2$, and λ must be real. So

$$\sigma_i = 0.$$

That is, $\sigma = 0$ for neutral stability.

EFFETS DE L'EXTREMUM DE DENSITE ET DES CONDITIONS AUX LIMITES SUR LA STABILITE D'UNE COUCHE D'EAU HORIZONTALEMENT CONFINEE

Résumé—A partir d'une relation simple non linéaire pour la densité, l'effet de l'extrémum de densité sur l'apparition de l'instabilité thermique dans une couche d'eau horizontalement confinée et chauffée par le bas (à t_1) et refroidie au dessus (à t_2) est étudiée expérimentalement et analytiquement. Les résultats tant analytiques qu'expérimentaux montrent que l'extrémum a pour effet de stabiliser la couche fluide. Les effets des conditions aux limites sont étudiés. L'analyse montre que les conditions aux limites réalistes (surfaces limites à capacité thermique finie) tendent à destabiliser, que les effets d'extrémums de densité soient ou non pris en compte. Néanmoins le comportement qualitatif de Ra_c avec $R = (t_m - t_2)/(t_1 - t_2)$ est relativement indépendant des conditions aux limites. L'effet combiné de l'extrémum de densité et des conditions aux limites réalistes est de destabiliser (par rapport à la limite de Boussinesq de $Ra_c = 1708$) pour des valeurs élevées de R, et de stabiliser, par quantités progressivement plus grandes, lorsque R augmente. Des modes initiaux différents d'instabilités pour des températures de surface supérieures ou inférieures à 4°C sont observés à l'aide d'un système Schlieren.

Les longueurs d'onde des formes distinctes de perturbation sont en bon accord avec celles calculées.

DER EINFLUSS DES DICHTEEXTREMUMS UND DER RANDBEDINGUNGEN AUF DIE STABILITÄT EINER HORIZONTAL BEGRENZTEN WASSERSCHICHT

Zusammenfassung—Mit einer einfachen nichtlinearen Beziehung für die Dichte wurde der Einfluß des Dichteextremums auf das Einsetzen der thermischen Instabilität in einer horizontal begrenzten Wasserschicht, die von unten beheizt (mit t_1) und von oben gekühlt (mit t_2) wird, experimentell und analytisch untersucht. Die analytischen und experimentellen Ergebnisse zeigen, daß das Dichteextremum eine stabilisierende Wirkung auf die Flüssigkeitsschicht hat. Der Einfluß der Randbedingungen wurde ebenfalls untersucht. Dabei zeigte sich, daß realistische Randbedingungen (angrenzende Oberfläche mit endlicher Wärmekapazität) mit und ohne Einfluß des Dichteextremums eine Destabilisierung begünstigen. Das qualitative Verhalten von Ra_c mit $R = (t_m - t_2)/(t_1 - t_2)$ ist jedoch relativ unabhängig von den Randbedingungen. Der Einfluß von beiden, dem Dichteextremum und den realistischen Randbedingungen, ist eine Destabilisierung für große negative R (in Bezug auf die Boussinesq Grenze von $Ra_c = 1708$) und eine Stabilisierung um allmählich größere Beträge, wenn R zunimmt. Verschiedene anfängliche Arten der Instabilität wurden bei Oberflächentemperaturen über und unter 4°C mit einem Schlierenverfahren beobachtet. Die Wellenlängen der beobachteten deutlichen Störungsformen stimmen gut mit den berechneten Wellenlängen überein.

ВЛИЯНИЕ ЭКСТРЕМАЛЬНОГО ЗНАЧЕНИЯ ПЛОТНОСТИ И ГРАНИЧНЫХ УСЛОВИЙ НА УСТОЙЧИВОСТЬ ГОРИЗОНТАЛЬНОГО СЛОЯ ВОДЫ

Аннотация—При помощи простого нелинейного соотношения для плотности проведено как теоретическое, так и экспериментальное исследование влияния экстремального значения плотности на начало неустойчивости горизонтально ограниченного слоя воды, нагреваемого сверху (при t_1) и охлаждаемого снизу (при t_2). Как аналитические, так и экспериментальные результаты показывают, что экстремальное значение плотности обладает эффектом стабилизации слоя жидкости. Рассматривается также влияние граничных условий. Анализ показывает, что реальные граничные условия (конечная теплоемкость граничащих поверхностей) ведут к дестабилизации как в случае включения эффекта экстремальной плотности, так и без него. Однако, качественное поведение Ra_c с $R = (t_m - t_2)/(t_1 - t_2)$ относительно независимо от граничных условий. Совместное действие как максимума плотности, так и реальных граничных условий при больших отрицательных R должно приводить к дестабилизации (относительно предела Буссинеска $Ra_c = 1708$), а с ростом R – к стабилизации. С использованием системы Шлирена наблюдались различные начальные моды неустойчивости температур поверхности при температур как выше, так и ниже 4°C. Длины волн наблюдаемых четких форм возмущений хорошо согласуются с рассчитанными длинами волн.